



# Evaluation of digital pulse processing techniques for a $\beta$ - $\gamma$ coincidence counting system

M. Teresa Durán<sup>\*</sup>, Youcef Nedjadi, Frédéric Juget, François Bochud, Claude Bailat

Institute of Radiation Physics (IRA), Lausanne, Switzerland

## ARTICLE INFO

### Keywords:

Digital pulse processing (DPP)  
Digital filters  
Digital coincidence counting (DCC)  
 $\beta$ - $\gamma$  coincidence counting

## ABSTRACT

Signal processing is a core part of any electronic chain for radioactivity measurement systems and can influence measurement results drastically. A thorough study of the different alternatives for this treatment is especially worthwhile when developing a new digital system.

This article describes an evaluation performed to optimize the digital pulse processing stage of the  $\beta$ - $\gamma$  coincidence counting system at the Institute of Radiation Physics (IRA) designated laboratory for the activity unit. This study is a part of IRA's digitalization project to modernize the aging analog electronic hardware of its primary measurement systems.

The  $\beta$ - $\gamma$  coincidence counting system consists of a plastic scintillation detector in the beta channel and a well-type NaI detector in the gamma channel. Six pulse shaping digital filters along with amplitude calculation algorithms were implemented to obtain beta and gamma pulse amplitude values. In addition, four timing digital filters and time pick-off methods were set up to calculate arrival times (timestamps) for the pulses generated by both detectors.

Filter parameters and algorithm settings were adjusted to obtain the best performance. Combination of filters into traditional two channel (fast for timing and slow for shaping) or one channel configuration using dCFD (digital constant fraction discrimination) and LE (leading edge) time pick-off methods were also tested and compared to study the *whole* digital pulse processing system, using both real measurement signals ( $^{241}\text{Am}$ ,  $^{137}\text{Cs}$ ,  $^{60}\text{Co}$  and  $^{166\text{m}}\text{Ho}$ ) and simulated reference pulses. The results of these tests were quantified by evaluating the following metrics: processing speed, signal-to-noise ratio (SNR) at different energies, gamma energy resolution, time measurement accuracy, time resolution and detection efficiency. The results of this evaluation provide a rational ground to assess the system and help decide which digital pulse processing (DPP) method should be the most appropriate.

## 1. Introduction

One of the critical stages when implementing an electronic digital system for activity measurements is the digital pulse processing stage. Digital pulse processing is the numerical analysis of the pulses provided by a radiation detector in order to obtain pulse properties such as amplitude and arrival time (timestamp) (Grzywacz, 2003). This analysis is performed using digital filters to replace analog pulse shaping and numerical algorithms to detect the pulses delivered by the filters and calculate their figures of interest.

The flexibility of this digital approach offers a wide range of possibilities in terms of digital filters to apply, along with the selection of their parameters, and the complementary algorithm implementation

using different methods for pulse detection, pulse height determination and time pick-off. In this situation, the choice of all elements for an optimal analysis turns out to be quite complex due to the wide offer to deal with and the criticality of the results obtained from the chosen configuration. Therefore, testing and evaluating the critical parameters (JRC, 2014) becomes an important step when designing and implementing a digital electronic system.

This paper describes the study of several DPP techniques by measuring and evaluating some critical parameters to find the best-suited configuration for the laboratory's  $4\pi\beta$ - $4\pi\gamma$  coincidence counting system.

First, the detection system and the electronic digital system are described, as well as the pulse simulator programmed to generate pulse

<sup>\*</sup> Corresponding author.

E-mail address: [teresa.duran@chuv.ch](mailto:teresa.duran@chuv.ch) (M.T. Durán).

<https://doi.org/10.1016/j.apradiso.2020.109100>

Received 27 March 2019; Received in revised form 17 February 2020; Accepted 24 February 2020

Available online 27 February 2020

0969-8043/© 2020 Elsevier Ltd. All rights reserved.

trains that correspond to certain characteristics of interest. A brief description of the digital acquisition stage is also included to describe the sampling process prior to the DPP stage.

Next, the implementation of digital shaping and timing filters is presented together with the algorithms for pulse detection, pulse height analysis and time pick-off methods.

Afterwards, the metrics and their evaluation methods are described, followed by the results obtained from  $^{241}\text{Am}$ ,  $^{137}\text{Cs}$ ,  $^{60}\text{Co}$  and  $^{166\text{m}}\text{Ho}$  source measurements and simulated pulse trains depending on the case.

Finally, the conclusions drawn from this study are presented.

## 2. Instruments and methods

### 2.1. Detectors

The counting system consists of a  $\beta$  plastic scintillation detector inserted into the well of a NaI(Tl) well-type  $\gamma$  detector.

The  $\beta$ -detector consists of a cylindrical plastic scintillator (UPS-89 or UPS-923A) with a dry radioactive source in its center. The scintillator is optically coupled to the window of a Photonis XP3132 low-noise photomultiplier tube (PMT). This instrument is inserted into the well of a Quartz & Silice 127-SPE-127 12.5 cm  $\times$  12.5 cm NaI(Tl) detector, coupled to a RTC type XP2050 photomultiplier. The whole detection system is kept inside a lead shielding to reduce background radiation. More detailed descriptions can be found elsewhere (Nedjadi et al., 2010), (Nedjadi et al., 2012) and (Durán et al., 2018).

The preamplifying stage consists of a Canberra 2005 charge-sensitive preamplifier in the  $\beta$  channel. In the  $\gamma$  channel, the detector output is connected to a dedicated module designed by J. Bouchard (Bobin et al., 2014) at LNHB (Laboratoire National Henri Becquerel - France) specially for NaI(Tl) detectors that process saturated pulses (mainly from cosmic origin and some from piled-up pulses) by a clamp amplifier reducing its amplitude to the input constraints of data acquisition systems (Keightley et al., 2013). Nevertheless, due to the small input voltage range of our digital system (2 V peak-to-peak) a voltage attenuator has to be added at the output of the preamplifying stage from each channel.

### 2.2. Pulse train simulator

Simulation of pulse trains was also needed to measure certain timing characteristics and the detection efficiency, as will be detailed below. To this purpose, a LabVIEW™ application was created to simulate realistic  $\beta$  and  $\gamma$  pulse trains with similar noise levels and selectable amplitude and rate following the Poisson distribution.  $\beta$  and  $\gamma$  pulse shapes were modeled using biexponential functions with typical rise and fall times for each detector-preamplifier configuration of the corresponding channel. Rates were selected ranging from  $10^3$  to  $10^6$  s $^{-1}$  and chosen as the mean value of the Poissonian probability distribution to generate the pulses. The amplitude of each pulse was generated randomly within the input voltage scale of the digitizer module (0–1 V). A white noise component was added with a similar noise level to that of the real detection electronic chain.

### 2.3. Digital system

IRA primary measurements laboratory's digital system is a National Instruments (NI) device composed of a high-bandwidth chassis (NI PXIe-1085) with an embedded processor (NI PXIe-8880). The chassis accommodates a double input digitizer adapter module (NI 5772) linked to a Kintex-7 FPGA (NI PXIe-7975R) that samples both channels at 100 MS/s<sup>1</sup> with a 12 bit resolution each. The acquired data are streamed to an external hard-drive RAID (redundant array of inexpensive disks) for

storage (NI HDD-8266). This transfer can be made at up to 3.6 GB/s thanks to a high-bandwidth connection (NI PXIe-8384). A timing and synchronization control card (NI PXIe-6672) ensures operating synchronicity and high precision timing due to a 10 MHz oscillator clock. This clock is calibrated on a regular basis using a 100 MHz traceable frequency.

The system is programmed with LabVIEW™ (NI). This system-design platform and development environment software allows control of the digital electronic system as well as data processing and analysis.

Fig. 1 depicts a schematic diagram of the whole  $4\pi\beta$ - $4\pi\gamma$  coincidence counting system including connections to the digital system (Durán et al., 2018) (see Fig. 2)

#### 2.3.1. Data acquisition

Data acquisition is performed by means of the FPGA embedded in the digitizer module and therefore the programming is done under a dedicated LabVIEW™ FPGA. The raw data acquired are directly streamed to a hard disk drive where they are stored until further processing configuring an “offline analysis” operation scheme.

Data are sampled at 100 MS/s, which corresponds to a 10 ns time resolution. This resolution allows a correct registration of the pulse rising edge (the most restrictive parameter) in order to calculate the pulse arrival time precisely (Durán et al., 2018). Typical fast rise times for the  $\beta$  pulses at the preamplifier output are around 100 ns, so at this sampling rate they are represented with 10 points.

A DMA (Direct Memory Access) FIFO (First-In, First-Out) structure and TDMS (Technical Data Management Streaming) files which permit writing data in parallel were used to stream the data to the hard-disk drive enhancing the speed of the whole process. Information from both  $\beta$  and  $\gamma$  input channels are stored as a single list of values (with 32-bit resolution) that must be decoded from the ADC code to voltage, taking into account the 12-bit resolution per channel and the  $\pm 1$  V dynamic range of the digitizer.

Once decoded, a list of voltage values (pulse train) with a time interval of 10 ns is obtained for each channel. This is the information the DPP algorithms have to process.

A scheme of the data acquisition structure is presented in the following figure:

## 3. Digital pulse processing implementation

Once the data is acquired, the main information to extract from each channel is pulse height and timestamp. To obtain this information, the process follows four steps: signal treatment by digital filtering, pulse detection, pulse timing and pulse height analysis.

### 3.1. Signal treatment by digital filters

As with the analogue electronics, signal treatment provides an appropriate input for pulse detection, timing and height analysis. Changing the shape of the pulses from the preamplifier allows a better pulse detection and discrimination by reducing pulse pile-up while preserving the information carried by the amplitude of the pulse (Knoll, 2000).

In the digital approach, this task is most often performed by the application of digital filters. In this paper, digital filters are classified into timing and shaping, depending on the information extracted from them. Timing filters are used to trigger the pulse analysis and calculate pulse timestamps. Shaping filters are used to perform pulse height analysis to obtain the pulse amplitude. This would be the two-channel or slow-fast procedure for pulse processing (CAEN, 2011) where a fast timing and a slow shaping filters are implemented in parallel. There is also another configuration where the shaping filter is used for both pulse height analysis and calculation of the pulse arrival time through LE (Leading Edge), dCFD (digital Constant Fraction Discrimination) and some other time pick-off methods (Streun et al., 2002), (Nelson et al.,

<sup>1</sup> S/s means samples per second.

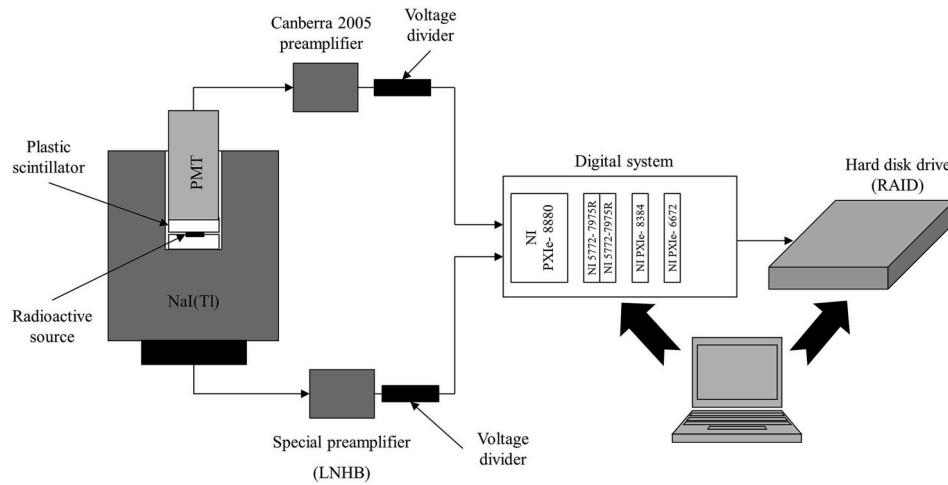


Fig. 1. Schematic diagram of the  $4\pi\beta$ - $4\pi\gamma$  coincidence counting with digital acquisition, processing and analysis system.

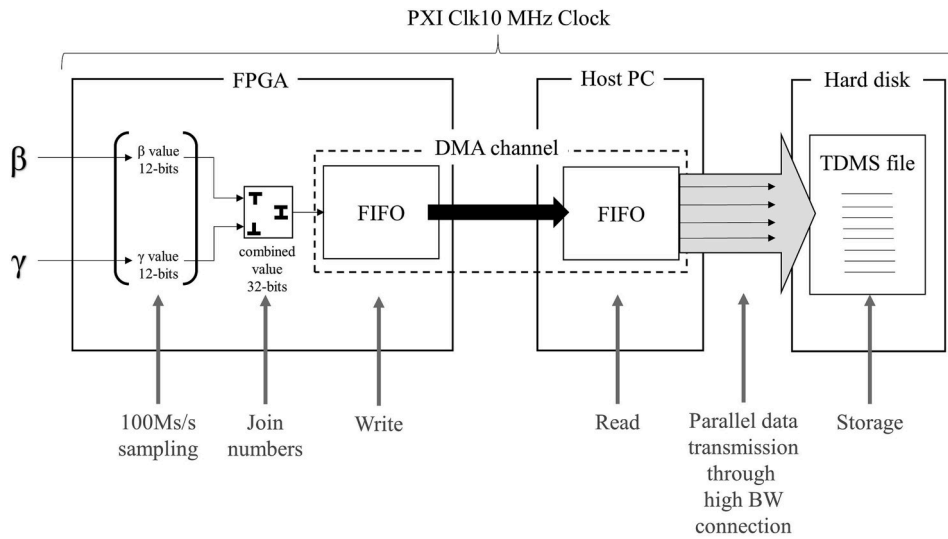


Fig. 2. Scheme of the acquisition, streaming and storage of measurement data.

2003), (Nakhostin, 2008), (Hu et al., 2010), (Aycak et al., 2010), (Jäger and Butz, 2012) and (Kamleitner et al., 2014). In this study, LE and dCFD were implemented to extract pulse timestamps from the shaping filter output signals.

### 3.2. Shaping filters

Whenever a shaping filter is applied, the original shape of the pulse must be taken into account in the implementation of the filter. The filter transfer function  $H(z)$  has to be calculated considering the input pulse shape, so it can be transformed into the desired shape successfully. In the case of preamplifier pulses with a long exponential decay tail, this feature has to be corrected by means of a pole-zero cancellation procedure. When detectors have a slower response, as in the case of NaI(Tl), a longer pulse rise time has to be considered for correction. This operation can be implemented following different approaches (Nakhostin, 2018). In our LabVIEW™ code, we have tested several configurations and our conclusion is that the implementation that requires less computational effort consists of two steps: first, the preamplifier pulses are converted into a steplike pulse (Fig. 3), and secondly the shaping filter is applied to obtain the step response. With this implementation, transfer functions for the steplike pulse and for the shaping filter applied are less complex.

The transfer functions for the transformations into a steplike pulse are:

$H(z) = \frac{1-\beta z^{-1}}{1-z^{-1}}$ , to transform an exponential decay pulse into a step function, where  $\beta = e^{-T/t_d}$  with  $T$  as the sampling interval and  $t_d$  is the decay time constant.

$H(z) = \frac{1-(\alpha+\beta)z^{-1}+\alpha\beta z^{-2}}{(\beta-\alpha)(1-z^{-1})}$  transforms a biexponential pulse into a step function, where  $\alpha = e^{-T/t_r}$  with  $t_r$  as the rise time constant.

The following six shaping filters were implemented: CR-(RC)<sup>4</sup> (Nakhostin, 2011), Gaussian (Bobin et al., 2014; Young and Van Vliet, 1995), Triangular, Cusp, Flat-top cusp and Trapezoidal (Jordanov and Knoll, 1994). The table below (Table 1) shows their transfer function and appearance for both beta and gamma channels.

#### 3.2.1. Timing filters

Timing filters are used for triggering as they perform baseline correction, eliminate high frequency noise and correct for low frequency fluctuations (CAEN, 2011). Pulses are transformed into bipolar signals in which the zero crossing point is independent from the pulse amplitude, so it can be used to mark the timestamp for the pulse.

Four timing filters were implemented for the beta and gamma channels. Gaussian (Young and Van Vliet, 1995), Moving average plus

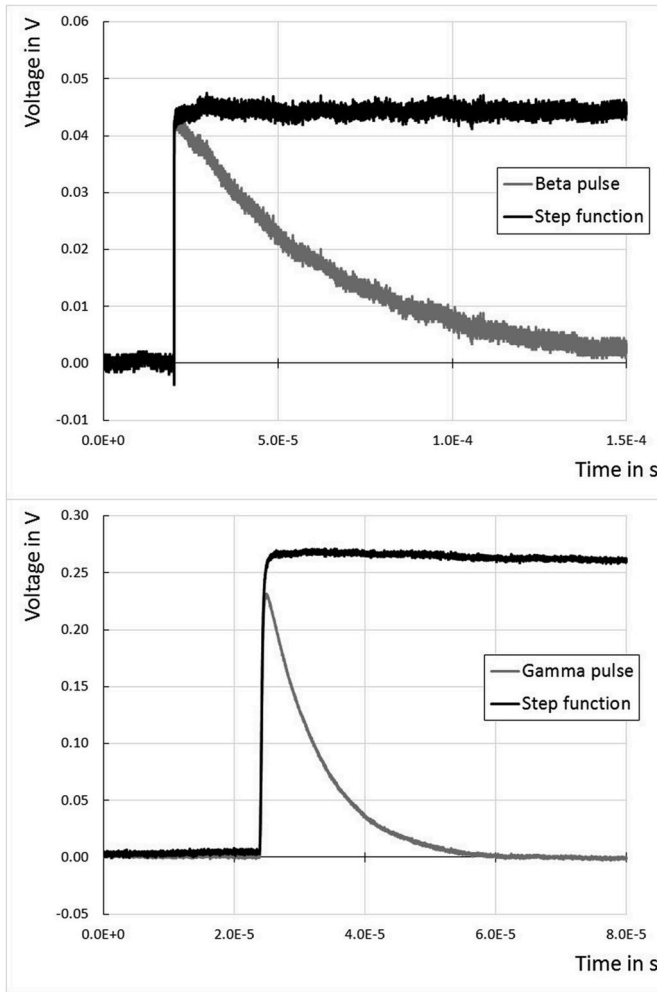


Fig. 3. Transformation result from original exponential decay beta pulse (upper) and biexponential gamma pulse (lower) to a steplike pulse.

double derivative (MA + DD) (Guzik and Krakowski, 2013), CR-RC-CR and RC-(CR)<sup>2</sup> based in (Nakhostin, 2011) filters are presented in the following graphs (Fig. 4) and their transfer functions are compiled in Table 2.

### 3.3. Pulse detection

Pulses are detected by threshold surpassing on the filtered signals. A threshold value is set over the high frequency noise level. Whenever the signal exceeds this value, pulse timing and pulse height analysis are triggered. To reduce false positives and treat saturated pulses, additional conditions are applied such as minimal and maximal pulse amplitudes respectively. Pile-up rejection is solved by the imposition of a veto window that prevents from triggering a new analysis during the time needed for the filters to produce a proper pulse shape to be analyzed.

### 3.4. Pulse timing

Pulse timing can be performed by different time pick-off methods based either on analog methods or on pure digital techniques (Nakhostin, 2018). Here, three methods were implemented.

#### 3.4.1. Zero-crossing method

This method applies a timing filter to the original pulse, which is transformed into a bipolar pulse as seen in Fig. 4. The point where the bipolar pulse crosses the horizontal axis (zero amplitude) is settled as the

timestamp of the pulse. This point is independent of the amplitude of the pulse, thus reducing inaccuracy due to amplitude walk (Knoll, 2000).

#### 3.4.2. Leading edge method (LE)

This method is the simplest, as it just calculates the time at which the signal crosses a certain threshold level. When the threshold does not match the signal samples, a linear interpolation is performed to obtain the timestamp value. This algorithm is applied to the output of the shaping filter, so that the baseline is already corrected from the pre-amplifier output signal and the high frequency noise is reduced to prevent false pulse detection. The threshold value is set over the amplitude level of this high-frequency noise.

#### 3.4.3. Digital constant fraction discriminator (dCFD)

The same principle of constant fraction discriminator (CFD) can be applied in the digital regime with no need to produce a bipolar pulse but using the preamplifier pulse or output pulse from the shaping filter instead (Nelson et al., 2003) (Nakhostin et al., 2008). The method calculates the amplitude of the pulse, searches for the fraction of the maximum and calculates the time at which this level is reached by linear interpolation in case it does not match a digitized value.

### 3.5. Pulse height analysis

Pulse height analysis is performed differently depending on the shape of the top of the pulse: flat, as in the case of trapezoidal and flat-top cusp filters, or not flat, as in the case of the rest of the shaping filters. When the top is flat, a mean value is calculated taking a few points from the central zone of the flat top. When there is no flat top, the algorithm simply looks for the maximum value. Baseline correction is always performed by subtracting from the maximum a mean value calculated taking various points before the pulse rising. As previously stated, pulse pile-up is solved by the imposition of a veto window.

## 4. Description of metrics and evaluation methods

The evaluation and comparison between the filters' performances is carried out using different metrics on simulated and experimental signals. Simulated signals are used when certain characteristics in emission rate and time stamping are needed: for time accuracy and detection efficiency evaluation. For the rest of the evaluations, experimental signals are used.

### 4.1. Processing speed

Processing speed can be an important parameter when designing a digital filter. It also gives an indication of the computational complexity of the algorithm. Experimental  $\beta$  and  $\gamma$  signals of the same duration were processed by each filter and their processing time was measured for similar gain and timing constant amongst the filters, so that the values are comparable.

### 4.2. Signal-to-noise ratio


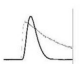
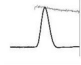





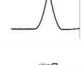



Signal-to-noise ratio (SNR) was measured at the output of the digital filters to serve as a comparative value between filter responses to noise. The following expression was used to calculate SNR:

$$SNR_{dB} = 10 \cdot \log \left[ \left( \frac{RMS_{signal}}{RMS_{noise}} \right)^2 \right]$$

where  $RMS_{signal}$  is the quadratic mean value of the signal amplitude, while  $RMS_{noise}$  is the quadratic mean value of the noise amplitude.

When considering pulses corresponding to high energy emissions, the SNR will be bigger than for pulses corresponding to low energy emissions. That is due to the different height of the pulses that will

**Table 1**  
Shaping filter transfer functions and output responses for beta and gamma pulses.

Filter	Transfer function	BETA PULSE SHAPE	GAMMA PULSE SHAPE
CR-(RC) <sup>4</sup>	$H(z) = \frac{\alpha T^3(4 - \alpha T)z^{-1} + \alpha^2 T^3(12 - 11\alpha T)z^{-2} - \alpha^3 T^3(12 + 11\alpha T)z^{-3} - \alpha^4 T^3(4 - \alpha T)z^{-4}}{24(1 - 5\alpha z^{-1} + 10\alpha^2 z^{-2} - 10\alpha^3 z^{-3} + 5\alpha^4 z^{-4} - \alpha^5 z^{-5})}$		
Gaussian	$H_1(z) = \frac{1 - z^{-1}}{b_0 - b_1 z^{-1} - b_2 z^{-2} - b_3 z^{-3}} H_2(z) = \frac{1}{B(b_0 - b_1 z^{-1} - b_2 z^{-2} - b_3 z^{-3})}$		
Triangular	$H(z) = \frac{1 - 2z^{-R} + z^{-2R}}{R(1 - z^{-1})}$		
Trapezoidal	$H(z) = \frac{1 - z^{-R} - z^{-(R+M)} + z^{-(R+M+R)}}{R(1 - z^{-1})}$		
Cusp	$H(z) = \frac{1 - z^{-(2k+1)} - (2k+1)z^{-k} + (2k+1)z^{-(k+1)}}{(1 - z^{-1})^2}$		
Flat-top cusp	$H(z) = \frac{1 - (k+1)z^{-k} + kz^{-(k+1)} - kz^{-l} + (k+1)z^{-(l+1)} - z^{-(l+k+1)}}{(1 - z^{-1})^2}$		

- CR-(RC)<sup>4</sup>:  $\alpha = 1/\tau$ ;  $\alpha = e^{-T/\tau}$ ;  $\tau = t/4$ ;  $T$  = sampling interval;  $t$  = time constant.
- Gaussian:  $b_i$  different polynomials in  $q$ , related to gaussian parameter  $\sigma$ ;  $B = 1/(b_1 + b_2 + b_3)/b_0$ , normalization constant.
- Triangular:  $R$  = triangle side length.
- Trapezoidal:  $R$  = trapezoid side length;  $M$  = trapezoid top length.
- Cusp:  $k$  = cusp side length.
- Flat-top cusp:  $k$  = cusp side length;  $l = k + m$ ;  $m$  = cusp top length.

therefore give a different  $RMS_{signal}$  value in each case. Then SNR was calculated at different energy levels for all filter outputs in beta and gamma channels, so that we could compare the performance of the filters when dealing with signals corresponding to different energy ranges.

#### 4.3. Energy resolution

The selection of the shaping filter is particularly important regarding the energy resolution in the gamma channel as the shaped pulse amplitude is related to energy. Flat-top pulse response filters tend to provide a better energy resolution (Salathe and Kihm, 2016) with a shorter shaping time than non-flat-top pulse response ones. Energy resolution has been measured for <sup>241</sup>Am (59.54 keV), <sup>137</sup>Cs (661.659 keV) and <sup>60</sup>Co (1173.24 keV) gamma total absorption peaks. Resolution was measured as the ratio between the FWHM (full width at half maximum) and the central energy of the peak expressed in percentage.

#### 4.4. Time resolution

To evaluate time resolution, histograms of the time intervals between  $\beta$  and  $\gamma$  consecutive events were performed using different filter and time pick-off methods. The smaller the difference, the higher the capacity to detect coincident events. This evaluation was made using the data acquired from the measurement of a <sup>166m</sup>Ho source.

#### 4.5. Time accuracy

When performing coincidence counting, measurement of the pulse arrival time (timestamp) is a delicate and important part of the pulse processing system. To evaluate the accuracy of this measurement the application of filters and time pick-off methods were tested using simulated pulse trains. In this manner, pulses representing  $\beta$  and  $\gamma$  signals were generated at a defined frequency modulated with a Gaussian noise (JRC, 2014). Then the width of the peak in the time interval histogram was measured to see if it corresponds to the standard deviation set in the modulation.

#### 4.6. Detection efficiency

$\beta$  and  $\gamma$  pulse trains were simulated at different emission rates following Poisson probability distribution. The detected rate was measured and compared to the simulated one for different filters and pulse detection methods. It should be noted that no live-time nor dead-time corrections were applied when counting the events. Piled-up pulses were discriminated and counted up to a certain time range determined by the veto time-window imposed for the analysis of the pulses, which contributes to the dead-time account. As dead-time was not corrected, we lose track of this pile-up events that fall within this veto time-window. The absolute values for the efficiency are not relevant, and they are used as a mean to compare the pulse detection ability of the DPP configurations under study.

### 5. Results

#### 5.1. Processing speed

Fig. 5 present the mean processing speed value obtained when filtering 1 ms timeframes of a <sup>166m</sup>Ho source measurement. The filters have the same gain and time constant parameters so that the results can be comparable.

As seen in the graphs, the filters progress in speed in the same order for both beta and gamma pulses being the CR-(RC)<sup>4</sup> shaping filter and the Gauss timing the fastest.

The times showed can only be used for comparison purposes, as the values will depend on the computational speed of the system used.

#### 5.2. Signal-to-noise ratio

Signal-to-noise ratio was measured at the output of all shaping and timing filters applied to beta and gamma channels of real measurements. As previously stated, we measured the SNR for pulses representing different levels of energy. For that purpose, we measured several radioactive sources and selected pulses with amplitudes corresponding to the energy values of interest.

In the beta case, we measured a <sup>166m</sup>Ho source and high energy and



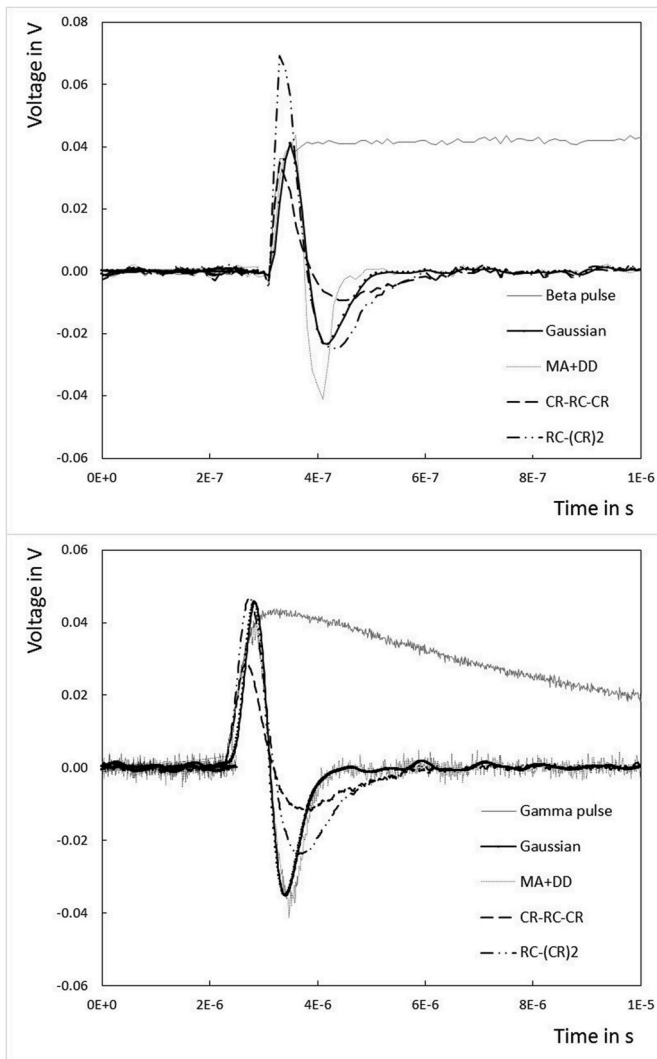


Fig. 4. Pulse response of the timing filters to real beta (upper) and gamma (lower) input pulses.

low energy levels were chosen.<sup>2</sup> For gamma measurements we chose the pulses corresponding to the emission energies of <sup>241</sup>Am at 54.5 keV, <sup>137</sup>Cs at 662 keV and <sup>60</sup>Co at 1173 keV. The following graphs show the results for shaping (Fig. 6) and timing filters (Fig. 7) with a gain of 1 and a time constant of 300 ns for  $\beta$  filters and 2  $\mu$ s for  $\gamma$  filters.

The results of SNR evaluation are consequent to the range of energies considered: the higher the energy, the bigger the ratio between signal and noise.

It is important to note that the SNR values are used to compare the performances of the filters and not to evaluate them independently. This means that the values themselves are not interesting to us; we only use them to compare performances regarding the noise. To that extent, the results are quite similar except for some outstanding cases that are detailed below.

For shaping filters, the Cusp filters has the lowest SNR value for both beta and gamma cases, with a maximum difference of around 5 and 4 dB respectively compared to best performance. The Triangular filter shows the best result for the beta case. For the gamma case, the best result changes with the energy range, but one may say that the best overall

<sup>2</sup> No energy calibration was performed for the beta spectrum. Low energy refers to the beginning of the beta spectrum and high energy refers to the spectrum tail.

Table 2  
Timing filter transfer functions.

Filter	Transfer function
Gaussian	$H_1(z) = \frac{1 - 2z^{-1} + z^{-2}}{b_0 - b_1z^{-1} - b_2z^{-2} - b_3z^{-3}};$ $H_2(z) = \frac{1}{B(b_0 - b_1z^{-1} - b_2z^{-2} - b_3z^{-3})}$
MA + DD	$H(z) = \frac{(1 - z^{-C})(1 - z^{-F})^2}{1 - z^{-1}}$
CR-RC-CR	$H_1(z) = \frac{a(1 - z^{-1})}{1 - az^{-1}}; H_2(z) = \frac{1 - b}{1 - bz^{-1}}; H_3(z) = \frac{c(1 - z^{-1})}{1 - cz^{-1}}$
RC-(CR) <sup>2</sup>	$H(z) = \frac{\alpha^2(1 + aT) - 2\alpha^2(1 + aT)z^{-1} + \alpha^2(1 + aT)z^{-2}}{(\alpha - z^{-1})^3}$

· Gaussian:  $b_i$  different polynomials in  $q$ , related to gaussian parameter  $\sigma$ ;  $B = 1/(b_1 + b_2 + b_3)/b_0$ , normalization constant.

· MA + DD:  $C$  = averaging points;  $F$  = differentiation constant.

· CR-RC-CR:  $a = \tau_1/(\tau_1 + T)$ ;  $b = \tau_2/(\tau_2 + T)$ ;  $c = \tau_3/(\tau_3 + T)$ ;  $\tau_1, \tau_2, \tau_3$  = filter time constants;  $T$  = sampling interval.

· RC-(CR)<sup>2</sup>:  $\alpha = 1/\tau$ ;  $\alpha = e^{-T/\tau}$ ;  $\tau = t/4$ ;  $T$  = sampling interval;  $t$  = time constant.

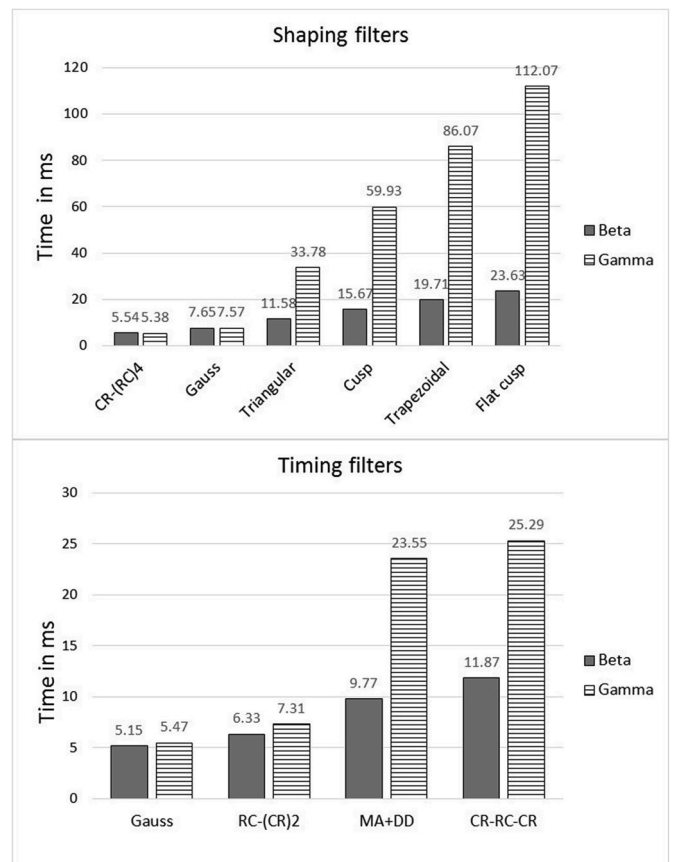


Fig. 5. Shaping (upper) and timing (lower) filter processing times in ms per ms of  $\beta$  and  $\gamma$  signal timeframes. Filter gain was 1 in all cases and time constants were 300 ns for beta filters and 2  $\mu$ s for gamma filters.

performance are those given by the CR-(RC)<sup>4</sup> and Gauss filters, as they show less dispersion of results between energy ranges.

With regard to the timing filters, the MA + DD filter shows a significantly lower performance in the gamma channel, almost 10 dB difference in the worst cases. This can be simply observed by looking at the outputs of the timing filters presented on the right side of Fig. 4. Gauss timing filter gives the best performance for beta signals and RC-(CR)<sup>2</sup> for gamma signals.

The SNR has an important impact on pulse sensing as it is done by threshold detection. The threshold level is going to be determined by the

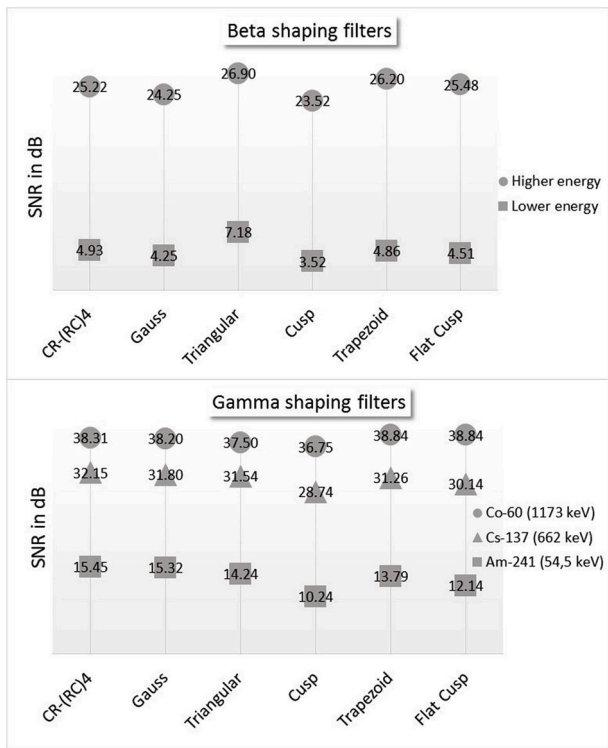


Fig. 6. Upper: SNR of beta shaping filter outputs for high and low energy pulses. Lower: SNR of gamma shaping filter outputs for pulses corresponding to  $^{241}\text{Am}$ ,  $^{137}\text{Cs}$  and  $^{60}\text{Co}$  typical emissions.

noise level: the lower the noise, the better the pulse sensing. Nevertheless, it is recommended, if possible, to rely on physical methods for noise reduction/removal than on electronic ones, as they are more reliable and stable over time.

### 5.3. Energy resolution

Resolution as the ratio of  $FWHM$  and central energy of the peak was measured for the total absorption peaks of  $^{241}\text{Am}$  and  $^{137}\text{Cs}$  obtained by applying the set of shaping filters with a gain of 1 and a time constant of 2  $\mu\text{s}$ . Fig. 8 shows the results in all cases:

The differences in energy resolution applying different shaping filters is very small, both for high and low energies. The NaI(Tl) well-type detector has a limited intrinsic energy resolution and, from the results showed, the use of different pulse processing systems does not improve it significantly. This is not the case for some other type of detectors, as in HPGe detectors, where the filters used to treat the pulses affect energy resolution considerably (Jornanov and Knoll, 1994) (Salathe and Kihm, 2016).

### 5.4. Time resolution

To study the time resolution a  $^{166\text{m}}\text{Ho}$  source was measured simultaneously with the  $\beta$  and  $\gamma$  detectors. Timestamps for each channel were calculated using the zero-crossing time pick-off method for the bipolar timing filter outputs and the time interval between consecutive  $\beta$  and  $\gamma$  events was calculated to show time resolution.

Another two time pick-off methods were developed using the shaping filter output: LE (leading edge) and dCFD (digital constant fraction discriminator). Shaping filters showing the maximum SNR value (not with flat-top because of their poor processing speed) were taken to implement LE and dCFD methods. To choose the fraction for the dCFD method, results for the time resolution using different fraction values were compared (Fig. 9).

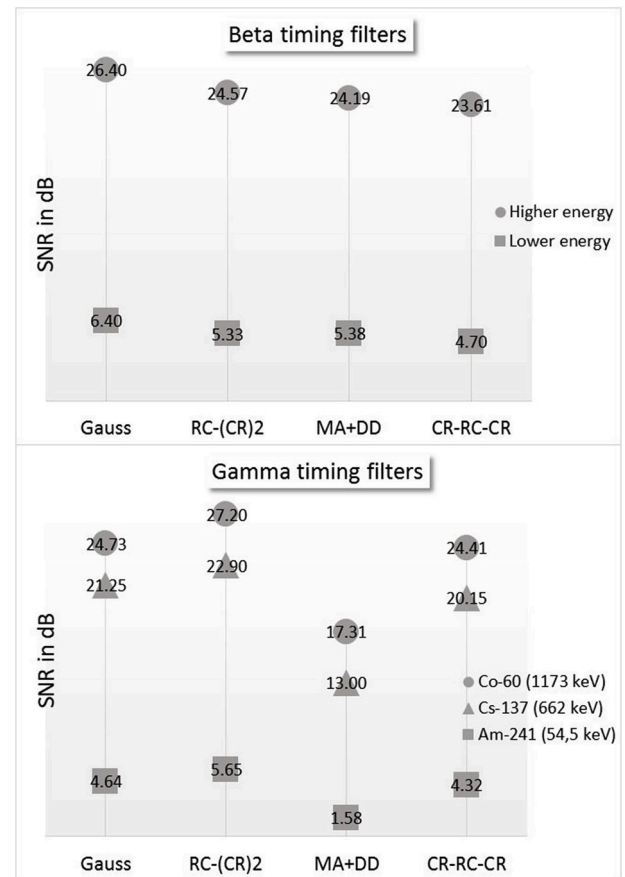


Fig. 7. Upper: SNR of beta timing filter outputs for high and low energy pulses. Lower: SNR of gamma timing filter outputs for pulses corresponding to  $^{241}\text{Am}$ ,  $^{137}\text{Cs}$  and  $^{60}\text{Co}$  typical emissions.

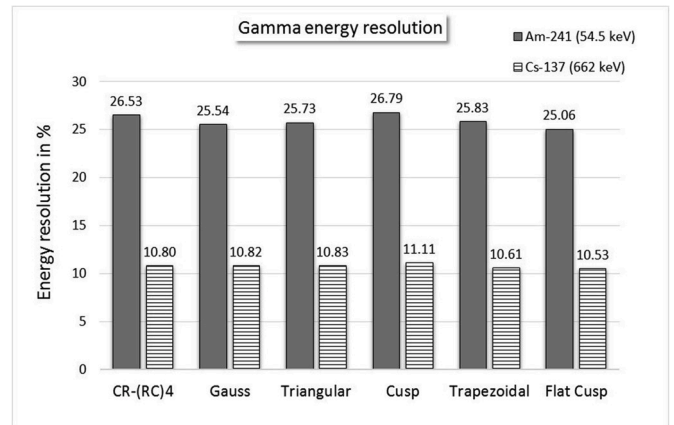


Fig. 8. Gamma energy resolution in percentage values for the total absorption peaks of  $^{241}\text{Am}$  and  $^{137}\text{Cs}$  using different shaping filters.

Fig. 10 shows the results for zero-crossing time pick-off with timing filters and LE and dCFD with fraction = 0.3 applied to the shaping filter outputs that showed the better SNR values in the previous section.

In the dCFD case, the fraction value is evaluated first to decide which one should be applied for the rest of the study. A fraction value of 0.3 gives the best time resolution (see Fig. 9).

It is clear that the dCFD method as well as LE consume much less processing time and resources than the zero-crossing one, as they only need one filter to resolve both amplitude and timestamp values and the

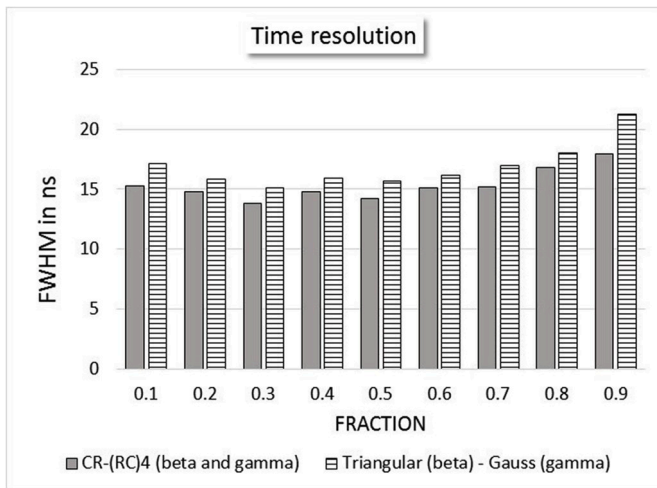


Fig. 9. FWHM (full width at half maximum) of  $\beta$ - $\gamma$  time intervals calculated using different fraction values for the dCFD method, combining CR-(RC)<sup>4</sup> shaping filters for  $\beta$  and  $\gamma$  channels and Triangular ( $\beta$ ) - Gauss ( $\gamma$ ).

calculations are simpler. Nevertheless, the LE edge method has a very poor time resolution compared to the other methods and is much more unstable because it is amplitude dependent, which may give incorrect timestamp values if the threshold is not well defined (Aykaç et al., 2010).

For the zero-crossing time pick-off method, the Gauss timing filter shows the lowest resolution.

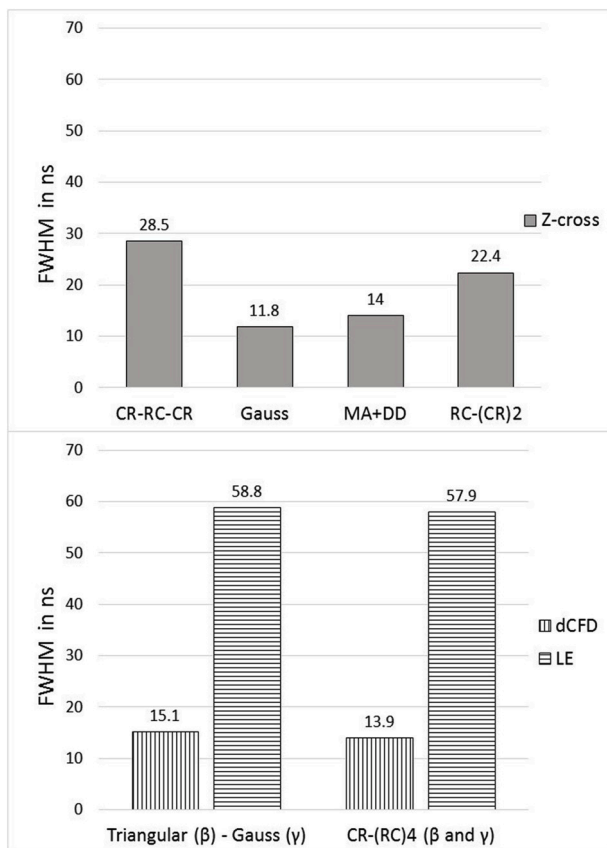


Fig. 10. Upper:  $\beta$ - $\gamma$  time interval histogram FWHM values for timing filters + zero-crossing time pick-off method. Lower: FWHM for shaping filters + dCFD (fraction = 0.3) and LE time pick-off methods.

### 5.5. Time accuracy

To test the time accuracy,  $\beta$  and  $\gamma$  pulse trains at 5 kHz and 20 kHz frequencies respectively, were generated introducing different levels of Gaussian noise in the frequency value. Timestamps were measured using different timing filters and time pick-off algorithms. Then the differences between consecutive timestamps were calculated to obtain the time interval histogram and its standard deviation. Fig. 11 shows the standard deviation values obtained with each filter and time pick-off method set for each simulated deviation ( $\sigma = 1\%$ , 10% and 30%) on the frequency value of the pulse train. dCFD stands for digital constant fraction discrimination and when not specified it means the zero-crossing method has been used.

The differences between the simulated and measured sigma values are under 5% in every case. For gamma pulses, the results are more accurate but less precise than for beta ones. Gamma pulses have a slower rise slope characterized by more points, which helps calculate the arrival time of the pulse with more accuracy than in the beta case. In both beta and gamma cases, zero-crossing time pick-off methods show a better overall accuracy than the dCFD method.

### 5.6. Detection efficiency

The following graphs (Figs. 12 and 13) show the detected rate using different combination of filters and time pick-off methods for simulated beta and gamma pulse train at various emission rates ranging from  $10^3$  s<sup>-1</sup> to  $10^6$  s<sup>-1</sup>.

Several filters and combinations were chosen in order to represent the filters that showed the better SNR values and gamma energy resolution as well as dCFD and zero-crossing time pick-off methods were

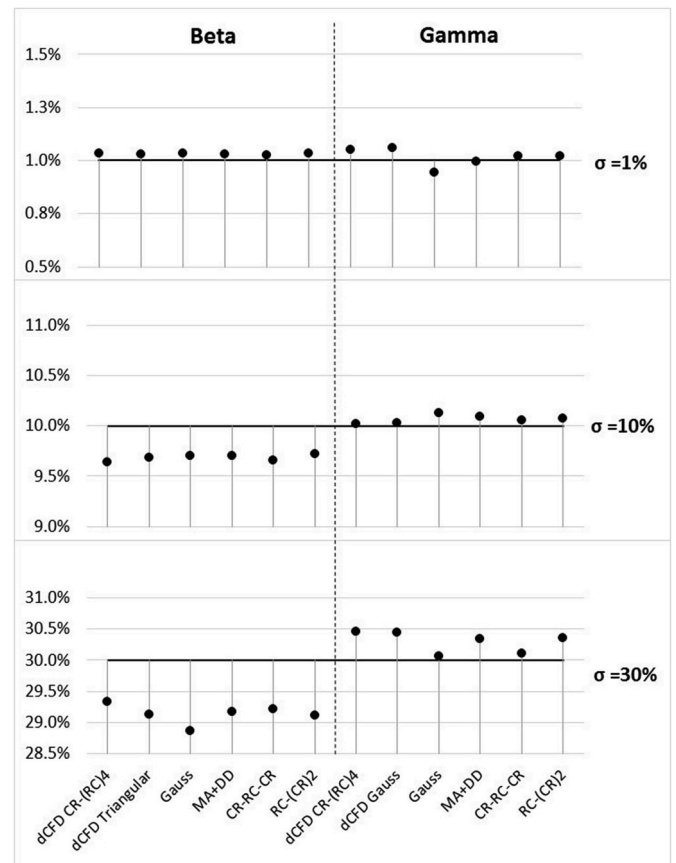
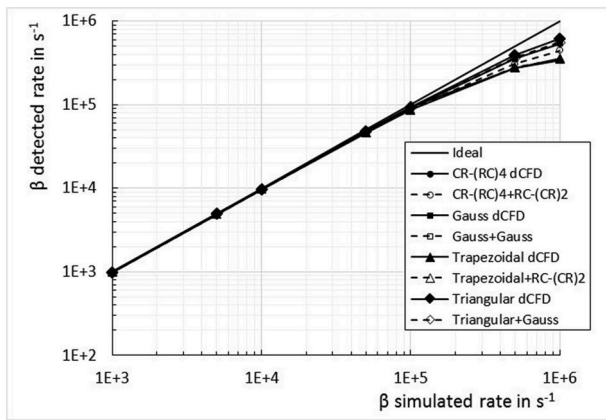


Fig. 11. Standard deviation in the measured frequency distribution for every filter and time pick-off method for simulated  $\beta$  and  $\gamma$  pulse trains at 5 kHz and 20 kHz mean frequency respectively.





**Fig. 12.** Beta detected rate versus simulated rate. When dCFD is indicated, it means that dCFD was applied to the mentioned shaping filter. Filter1+filter2 means Filter1 was used for pulse height analysis and filter2 for timestamp calculation using zero-crossing method.

applied to these filters to compare performances.

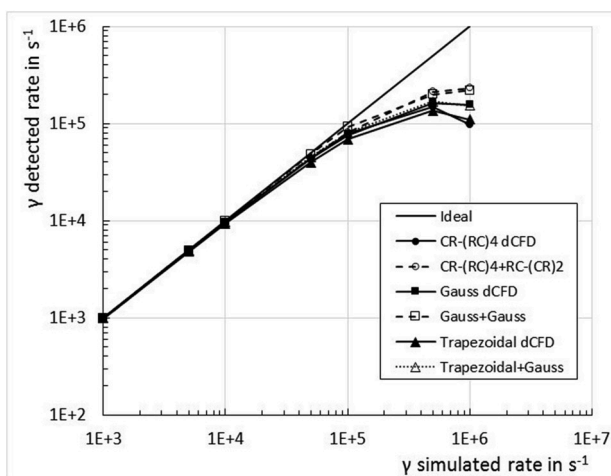
In the case of beta pulses, the performance is similar for all algorithms up to 50 kcps staying below 10% difference between simulated and detected rates. For higher rates, the results differ more widely between configurations and with respect to the simulated value. The top performance is achieved by the Triangular dCFD and Triangular + Gauss configurations probably due to their better SNR.

For gamma pulses, as they are slower, filters with longer shaping times are needed to treat them, resulting in a larger loss of events from rates of about 2 kcps, except for the Gauss + Gauss configuration, that shows a particularly good performance up to 100 kcps rates.

It should be noted that no dead-time compensation was applied to the detected rates and this certainly has an influence on the deviation of the detected from the simulated rate. Nevertheless the aim of this test was to obtain a simple metric to compare detection ability and the values should not be taken as a proper detection efficiency measurement result.

## 6. Conclusions

Digital pulse processing methods were described in detail, implemented and tested within a defined metrics and evaluation framework.



**Fig. 13.** Gamma detected rate versus simulated rate. When dCFD is indicated, it means that dCFD was applied to the mentioned shaping filter. Filter1+filter2 means Filter1 was used for pulse height analysis and filter2 for timestamp calculation using zero-crossing method.

This study was applied to a specific detection system giving particular results for their output pulses characteristics, but the method is applicable to any other detection system. When implementing a digital pulse processing configuration, it is necessary to evaluate its performance and this study describes the tools to accomplish this task.

This study shows that the results obtained for all the methods presented do not significantly differ when the filters are properly adapted to the input signals and the pulse height and arrival time calculation algorithms are correctly implemented.

The parameter that varies more drastically is the processing speed, especially for the slower gamma pulses: nearly a factor 20 between the slowest and the fastest shaping filters and a factor 5 for timing filters. Using dCFD or LE methods for time pick-off significantly reduces computational effort and time compared to zero-crossing method, as from only one filter application and simpler calculations the information of interest is obtained, but they present a reduced performance in terms of time accuracy and resolution.

In our particular case for the coincidence counting system described, the Gauss filters, both shaping and timing, give the best overall performance for gamma pulses. They are fast, show a good SNR, acceptable time accuracy and energy resolution and best detection efficiency. For beta pulses, the Gauss filters also give good general results, as well as the Triangular filter, that has the best SNR and a good detection efficiency when used with dCFD or combined with Gauss timing filter and zero-crossing time pick-off method.

Generally speaking, the choice of the filters and calculation methods will depend on the constraints of time, computing capacity, need for improved time or energy resolution and the range of the emission rate to measure. The importance of these parameters might change from one measurement to another, giving different results for the better digital pulse processing configuration to apply in each case.

## Declaration of competing interest

The authors declare that they have no known competing financial interests or personal relationships that could have appeared to influence the work reported in this paper.

## CRedit authorship contribution statement

**M. Teresa Durán:** Conceptualization, Methodology, Software, Validation, Formal analysis, Investigation, Resources, Writing - original draft, Visualization. **Youcef Nedjadi:** Conceptualization, Resources, Writing - review & editing. **Frédéric Juget:** Resources, Writing - review & editing. **François Bochud:** Writing - review & editing, Project administration. **Claude Bailat:** Writing - review & editing, Supervision.

## Appendix A. Supplementary data

Supplementary data to this article can be found online at <https://doi.org/10.1016/j.apradiso.2020.109100>.

## References

- Aycak, M., Inki, H., Sanghee, C., 2010. Timing performance comparison of digital methods in positron emission tomography. *Nucl. Instrum. Methods A* 623, 1070–1081.
- Bobin, C., Bouchard, J., Thiam, C., Ménesguen, Y., 2014. Digital pulse processing and optimization of the front-end electronics for nuclear instrumentation. *Appl. Radiat. Isot.* 87, 195–199.
- Caen, 2011. *Digital Pulse Processing in Nuclear Physics*, p. WP2081.
- Durán, M.T., Nedjadi, Y., Juget, F., Bochud, F., Bailat, C., 2018. Fast digital  $4\pi$ – $4\pi$  coincidence counting with offline analysis at IRA. *Appl. Radiat. Isot.* 134, 329–336.
- Grzywacz, R., 2003. Applications of digital pulse processing in nuclear spectroscopy. *Nucl. Instrum. Methods B* 204, 649–659.
- Guzik, Z., Krakowski, T., 2013. Algorithms for digital  $\gamma$ -ray spectroscopy. *Nukleonika* 58 (2), 333–338.

- Hu, W., Choi, Y., Hong, K.J., Kang, J., Jung, J.H., Huh, Y.S., Lim, H.K., Kim, S.S., Min, B. J., Kim, B.-T., 2010. A simple and improved digital timing method for positron emission tomography. *Nucl. Instrum. Methods A* 622, 219–224.
- Jäger, M., Butz, T., 2012. FPGA implementation of digital constant fraction algorithm with fractional delay for optimal time resolution. *Nucl. Instrum. Methods A* 674, 24–27.
- Jordanov, V.T., Knoll, G.F., 1994. Digital synthesis of pulse shapes in real time for high resolution radiation spectroscopy. *Nucl. Instrum. Methods A* 345, 337–345.
- JRC Technical Reports (various authors), 2014. Critical parameters and performance tests for the evaluation of digital data acquisition hardware. Report EUR 26976 EN.
- Kamleitner, J., Coda, S., Gnesin, S., Marmillod, Ph, 2014. Comparative analysis of digital pulse processing methods at high count rates. *Nucl. Instrum. Methods A* 736, 88–98.
- Keightley, J., Bobin, C., Bouchard, J., Capogni, M., Loreti, S., Roteta, M., 2013. Recent advances in digital coincidence counting for radionuclide metrology. In: *Proceedings of the 3rd International Conference on Advancements in Nuclear Instrumentation, Measurement Methods and Their Applications (ANIMMA)*.
- Knoll, G.F., 2000. *Radiation Detection and Measurement*, third ed. John Wiley & Sons, Inc.
- Nakhostin, M., Oishi, T., Baba, M., 2008. Time resolution measurement of avalanche counters using digital signal processing technique. *Radiat. Meas.* 43, 1493–1497.
- Nakhostin, M., 2011. Recursive algorithms for real-time digital CR-(RC)<sup>n</sup> pulse shaping. *IEEE Trans. Nucl. Sci.* 58 (5), 2378–2381.
- Nakhostin, M., 2018. *Signal Processing for Radiation Detectors*. John Wiley & Sons, Inc.
- Nedjadi, Y., Bailat, C., Caffari, Y., Bochud, F., 2010. Standardisation of <sup>18</sup>F by a coincidence method using full solid angle detectors. *Appl. Radiat. Isot.* 68, 1309–1313.
- Nedjadi, Y., Bailat, C., Bochud, F., 2012. Primary activity measurements with a 4 $\pi$  $\beta$ –4 $\pi$  $\gamma$  coincidence counting system. *Appl. Radiat. Isot.* 70, 249–256.
- Nelson, M.A., Rooney, B.D., Dinwiddie, D.R., Brunson, G.S., 2003. Analysis of digital timing methods with BaF<sub>2</sub> scintillators. *Nucl. Instrum. Methods A* 505, 324–327.
- Salathe, M., Kihm, T., 2016. Optimized digital filtering techniques for radiation detection with HPGe detectors. *Nucl. Instrum. Methods A* 808, 150–155.
- Streun, M., Brandenburg, G., Larue, H., Zimmermann, E., Ziemon, K., Halling, H., 2002. Coincidence detection by digital processing of free-running sampled pulses. *Nucl. Instrum. Methods A* 487, 530–534.
- Young, I.T., Van Vliet, L.J., 1995. Recursive implementation of the Gaussian filter. *Signal Process.* 44, 139–151.